

# Recovery of Iron-Dependent Autotrophic Denitrification Activity from Cell–Iron Mineral Aggregation-Induced Reversible Inhibition by Low-Intensity Ultrasonication

Tian Tian, Ke Zhou, Yu-Sheng Li, Dong-Feng Liu, and Han-Qing Yu\*



Cite This: *Environ. Sci. Technol.* 2022, 56, 595–604



Read Online

ACCESS |

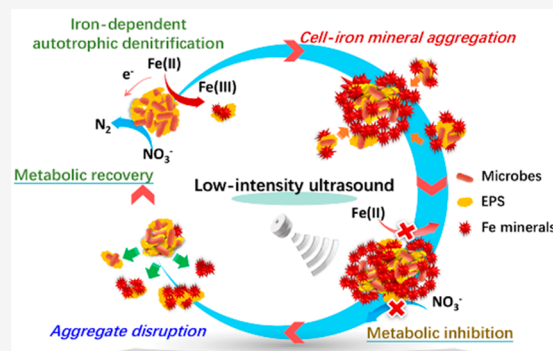
Metrics & More

Article Recommendations

Supporting Information

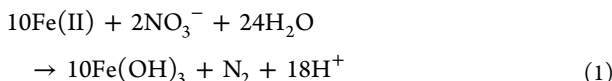
**ABSTRACT:** Iron-dependent autotrophic denitrification (IDAD) has garnered increasing interests as an efficient method for removing nitrogen from wastewater with a low carbon to nitrogen ratio. However, an inevitable deterioration of IDAD performance casts a shadow over its further development. In this work, the hidden cause for such a deterioration is uncovered, and a viable solution to this problem is provided. Batch test results reveal that the aggregation of microbial cells and iron-bearing minerals induced a cumulative and reversible inhibition on the activity of IDAD sludge. Extracellular polymeric substances were found to play a glue-like role in the cell–iron mineral aggregates, where microbial cells were caged, and their metabolisms were suppressed. Adopting low-intensity ultrasound treatment efficiently restored the IDAD activity by disintegrating such aggregates rather than stimulating the microbial metabolism. Moreover, the ultrasonication-assisted IDAD bioreactor exhibited an advantageous nitrogen removal efficiency (with a maximum enhancement of 72.3%) and operational stability compared to the control one, demonstrating a feasible strategy to achieve long-term stability of the IDAD process. Overall, this work provides a better understanding about the mechanism for the performance deterioration and a simple approach to maintain the stability of IDAD.

**KEYWORDS:** Iron-dependent autotrophic denitrification, low-intensity ultrasonication, cell-mineral aggregation, extracellular polymeric substances, cell encrustation, iron oxidation



## INTRODUCTION

In the last two decades, the microbially driven transformations of iron and nitrogen species and their functions in global biogeochemical cycles have been gradually unveiled.<sup>1,2</sup> Among these transformations, anoxic iron-dependent denitrification, also known as nitrate-dependent anaerobic iron oxidation, is one prominent representative.<sup>3,4</sup> In such a reaction, microorganisms can reduce nitrate with both ferrous ions and Fe(II)-bearing minerals as the sole electron donors (reaction 1). This process was first discovered by Straub et al.,<sup>5</sup> who isolated the original anoxic iron-dependent denitrifying consortia (named as the enrichment culture KS) from a freshwater sediment. The discovery of anaerobic iron-oxidizing denitrifiers broadens understanding of the iron and nitrogen cycles, particularly in oxygen-poor environments.<sup>2</sup>



Inspired by the anoxic iron-dependent denitrification in natural ecosystems, researchers have recently introduced such specific consortia and/or bacteria into bioremediation of contaminated environments, including *in situ* heavy metal

immobilization,<sup>6–9</sup> nitrogen removal coupled to phosphorus recovery,<sup>9–11</sup> and more. It is worth noting that the enrichment culture KS is convincingly recognized as neutrophilic chemolithoautotrophic microbial consortia.<sup>12,13</sup> Thus, iron-dependent autotrophic denitrification (IDAD) is well accepted as an emerging nitrogen removal technology and has attracted growing interests in treating wastewaters with low C/N ratios.<sup>15</sup> The enrichment culture KS is dominated by a strain from the family of Gallionellaceae, designated as the autotrophic Fe(II) oxidizer, while a flanking community including less abundant denitrifiers (e.g., *Rhodanobacter* sp., *Bradyrhizobium* sp.) drives nitrate reduction.<sup>12–14</sup> Recently, more autotrophic nitrate-reducing Fe(II)-oxidizing cultures have been enriched from natural aquifers.<sup>16,17</sup> Moreover, acclimation of the enrichment culture KS-like microbial

Received: August 17, 2021

Revised: November 26, 2021

Accepted: December 8, 2021

Published: December 21, 2021



consortia from activated sludge is also successively reported, providing a promising avenue for the application of IDAD.<sup>15,18,19</sup>

Unfortunately, in studies on IDAD, an unexpected performance deterioration in long-term operation has been recently reported,<sup>18–21</sup> which has considerably shadowed the development of IDAD. In these studies, the IDAD sludge after long-term cultivation was found to have clear morphological properties of association of microbial cells with Fe(III) precipitates.<sup>18–20</sup> Such cell–iron mineral aggregates are similar to the cell encrustation caused by iron minerals in mixotrophic Fe(II)-oxidizing denitrifying bacteria.<sup>22,23</sup> Cell encrustation indicates strong periplasmic or cytoplasmic iron accumulations, which are presumably induced by indirect Fe(II) oxidation via heterotrophic nitrate-reduction-derived nitrite.<sup>22,24</sup> The encrustation is suggested to pose a severe threat to cells by reducing cell motility, hindering metabolic activity, and even causing cell death.<sup>22</sup> Thus, it is recognized as the main cause for the deterioration of the IDAD bioreactor and the bottleneck for system sustainability of the IDAD process.<sup>18,19,25</sup>

However, so far there is still debate about whether such a cell encrustation exists in the IDAD process. Unlike mixotrophic Fe(II)-oxidizing denitrifying bacteria, the enrichment culture KS was reported to complete autotrophic Fe(II) oxidation without cell encrustation.<sup>13,24</sup> In these works, the iron minerals produced by Fe(II) oxidation were found to be mainly distributed outside cells<sup>24</sup> and closely associated with extracellular polymeric substances (EPS).<sup>22,24</sup> When fed with Fe(II), a larger amount of EPS (mainly containing proteins and polysaccharides) would be secreted by microorganisms to form microbial aggregates as a typical response against toxic metals.<sup>26</sup> For iron-oxidizing biosystems, the EPS–iron-mineral association is proposed as one potential mechanism for microorganisms to avoid encrustation of iron minerals.<sup>27,28</sup> For instance, the binding of iron minerals to EPS can effectively prevent the formation of relatively large-sized minerals and the cells enwrapped by these minerals.<sup>22</sup> But even then, it is clear that the iron minerals are continuously produced in IDAD bioreactors, and their binding with EPS as well as microbial cells is inevitable. If left unmanaged, the accumulation of these solid precipitates may form larger aggregates that retard the transport and uptake of substances, which is assumed as the hidden reason for the previously observed deterioration of IDAD bioreactors.<sup>1,15,20</sup> To disintegrate iron mineral-associated microbial aggregates, using low-intensity ultrasound to separate EPS or free cells from iron minerals seems to be an appropriate strategy. The purely mechanical effect of ultrasound can induce a stretching vibration of microbial aggregates, which will further disintegrate the substances that cover cells rather than destroy the intracellular structure.<sup>29,30</sup> Moreover, the dispersion effect of ultrasound is also reported to enhance the cellular permeability, thus favoring the nutritional transport as well as the microbial metabolism.<sup>31,32</sup> If the suppressed IDAD activity could be restored after ultrasonic treatment, the explanation of the cell encrustation-induced IDAD deterioration could be indirectly ruled out.

Therefore, this work aims to verify the above assumption. For this purpose, a continuous cyclic cultivation of IDAD sludge was conducted to explore the deterioration of the IDAD process. Also, the role of EPS in the formation of cell–iron mineral aggregates was investigated. Moreover, a low-intensity

ultrasound treatment was adopted to recover the metabolic activity of IDAD sludge. In the meantime, a ultrasonication-assisted IDAD bioreactor was built, and its stability was comparatively evaluated. These findings may deepen our understanding about the IDAD process and expand its application.

## MATERIALS AND METHODS

**IDAD Sludge and Cultivation.** The IDAD sludge used in the present work was collected from an acclimation bioreactor in our lab. The sludge was dominated by the genera of *Gallionellaceae*, *Caldilineaceae*, *Thermononas*, *Geothrix*, *Anaerolineaceae*, and *Nitrosomonadaceae*.<sup>15</sup> Among these genera, *Gallionellaceae* is mainly known as a microaerophilic Fe(II) oxidizer, and the others consist of a flanking community.<sup>12,13</sup> Details about the acclimation bioreactor were fully reported previously.<sup>11,15</sup> The IDAD sludge was anaerobically cultivated in a synthetic wastewater with sodium bicarbonate as the sole carbon source. NO<sub>3</sub><sup>−</sup>-N (sodium nitrate, 1–4 mM) and Fe(II) (ferrous sulfate, 5–12 mM) were supplemented as the electron acceptor and donor, respectively. Other compositions of the synthetic wastewater are shown in the Supporting Information.

**Cyclic Cultivation of IDAD Sludge.** To investigate the potential activity loss caused by the formation of cell–mineral aggregates, continuous cultivation of the IDAD sludge in a cycling mode was conducted in batch tests. First, the IDAD sludge withdrawn from the acclimation bioreactor was washed three times with deionized water to remove residual nutrients. Subsequently, the sludge was injected into the serum vials containing synthetic wastewater (100 mL, pH 7.0 ± 0.1) to a final mixed liquor suspended solids (MLVSS) of 800 mg/L. All vials were sealed with rubber stoppers and aluminum caps and flushed with high-purity N<sub>2</sub> for 20 min to maintain anoxic conditions. NO<sub>3</sub><sup>−</sup>-N (1.5 mM) and Fe(II) (8.0 mM) were added at a molar ratio of approximately 0.2. Sodium bicarbonate (0.5 g L<sup>−1</sup>) was supplemented as the inorganic carbon source in the cyclic cultivation. Finally, the serum vials were cultivated at 30 ± 1 °C in the dark, and liquid samples were collected at given time intervals to determine the concentrations of NO<sub>3</sub><sup>−</sup>-N and Fe(II). After each cycle, IDAD sludge samples were collected by three-fold centrifugation (8000 rpm, 10 min at 20 °C) plus washing with deionized water. Afterward, the washed sludge was injected again into the vials for the next cyclic cultivation. The batch tests contained four cycles, and each cycle lasted for 96 h. After four cycles of cultivation, the IDAD samples were collected from sacrificial vials to observe the sludge–iron mineral aggregates using scanning electron microscopy (SEM, JSM-6700F, JEOL Co. Japan).<sup>33</sup>

**Ultrasonic Treatment of IDAD Sludge.** The effect of low-intensity ultrasound on recovering the IDAD activity was immediately explored after four cycles of incubation. Briefly, the IDAD sludge was withdrawn and washed three times using deionized water, followed by addition into sterile vials containing fresh synthetic wastewater (100 mL). After sealing and deoxidizing (by bubbling N<sub>2</sub> for 20 min) treatment, the vials were treated in an ultrasonic cleaning bath (KQ-50ES, Kunshan Ultrasonic Instruments Co., China), which had a fixed frequency of 25 kHz and power of 50 W. The vials were partially immersed in the bath and fixed at the center of the support to maintain uniform ultrasonic irradiation. Time durations of 1, 2, 5, and 10 min were chosen to examine the recovery of IDAD activity. In addition, the potential

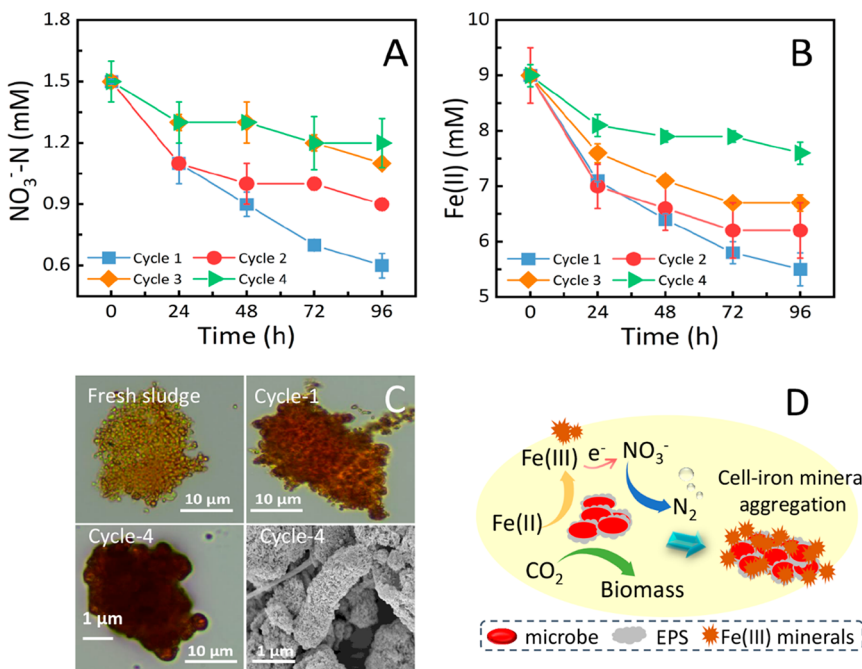


**Figure 1.** Activity loss of the IDAD sludge after four cycles of cultivation (A, B). Microscopy images and SEM images of IDAD sludge along with  $\text{Fe}(\text{II})$  oxidation (C) and proposed formation of cell–iron mineral aggregates (D). Error bars represent the standard deviations of the triplicate batch tests.

stimulation of IDAD activity by low-intensity ultrasound treatment with a fresh IDAD sludge was also evaluated as a compared amendment.

**EPS Analyses.** To investigate the role of EPS in the association of microbial cells and iron minerals, batch tests were conducted with either IDAD sludge or activated sludge as an inoculum according to the different experimental requirements. Briefly, a fresh IDAD sludge sample was injected into the vials containing synthetic wastewater (100 mL) under anoxic conditions. The EPS variation as well as the  $\text{Fe}(\text{II})$  oxidation and nitrate reduction in the IDAD process were measured. The EPS of the fresh IDAD sludge and the IDAD sludge at the end of batch tests were extracted and quantified. The EPS solution and the freeze-dried EPS powders were collected for three-dimensional excitation–emission matrix (EEM) fluorescence spectroscopy and Fourier transform infrared (FTIR) spectroscopy analyses, respectively. Fluorescence EEM spectra of the EPS were read from a LS55 luminescence spectrometer (PerkinElmer, Inc., USA). The FTIR spectra were recorded (NICOLET, iZ10, Thermo Scientific Co., USA) in a transmission mode with air as the background. Detailed parameters of the testing procedure were described previously.<sup>34</sup> Details regarding the activated sludge and the EPS extraction and quantification methods are described in the Supporting Information.

**Ultrasonication-Assisted IDAD Bioreactor.** Figure S1 shows the schematic diagram of two identical bench-scale up-flow anaerobic sludge blanket (UASB) bioreactors, which were constructed to investigate the potential assistance of low-intensity ultrasound to IDAD process. The bioreactors with a working volume of 0.8 L were operated in a continuous-flow mode with a hydraulic retention time (HRT) of 6 h for 120 days. The IDAD sludge from the acclimation bioreactor was used as the inoculum with an initial mixed liquor volatile suspended solid (MLVSS) concentration of approximately 2000 mg/L. The feeding (synthetic wastewater mentioned

above) was adjusted to an initial pH of  $7.2 \pm 0.1$  using 1.0 M HCl, and the dissolved oxygen (DO) levels in the reactors were maintained below 0.5 mg/L. An external ultrasonic generator (CE-5200A, PENGJU Co., China) was equipped to provide intermittent low-intensity ultrasound (50 W, 60 kHz) to the bioreactors. For ultrasonic treatment, the ultrasound was given at the very beginning of each phase for 5 min. The continuous operation of IDAD bioreactors was divided into four phases based on different sonication durations, and the details of each phase are summarized in Table S1.

**Chemical Analysis.** DO and pH were measured using a portable DO meter (HQ30d, HACH Co., USA) and a benchtop pH meter (FE-28, Mettler-Toledo Inc., USA), respectively. The influent and effluent samples were collected and analyzed after being filtered with a 0.22-μm-pore poly(ether sulfone) filter for concentrations of  $\text{NO}_3^-$ -N and  $\text{NO}_2^-$ -N using the standard methods.<sup>35</sup> Fe, including  $\text{Fe}(\text{II})$  and total Fe, was determined by the phenanthroline assay.<sup>36</sup> Batch tests were conducted in triplicate, and the results are expressed as the mean  $\pm$  SD. Statistical analysis was carried out using one-way ANOVA with Duncan's multiple range test (SPSS 19.0), and values of  $p < 0.05$  were considered statistically significant.

## RESULTS

**Activity Loss of IDAD Sludge in Cyclic Cultivation.** In iron-dependent denitrification, the  $\text{Fe}(\text{II})$  oxidation provides microorganisms with electrons to reduce nitrate to nitrogen intermediates (e.g., nitrite, nitric oxide, and nitrous oxide) and finally to  $\text{N}_2$ . Thus, the encapsulation of microbes by the poorly soluble iron products is inevitable under such circumstances. As a result, the aggregation of cells and iron minerals is supposed to be an adverse factor affecting microbial activity in iron-dependent denitrification<sup>18,24</sup> and in other iron-involved biological treatment processes.<sup>37</sup> To demonstrate the

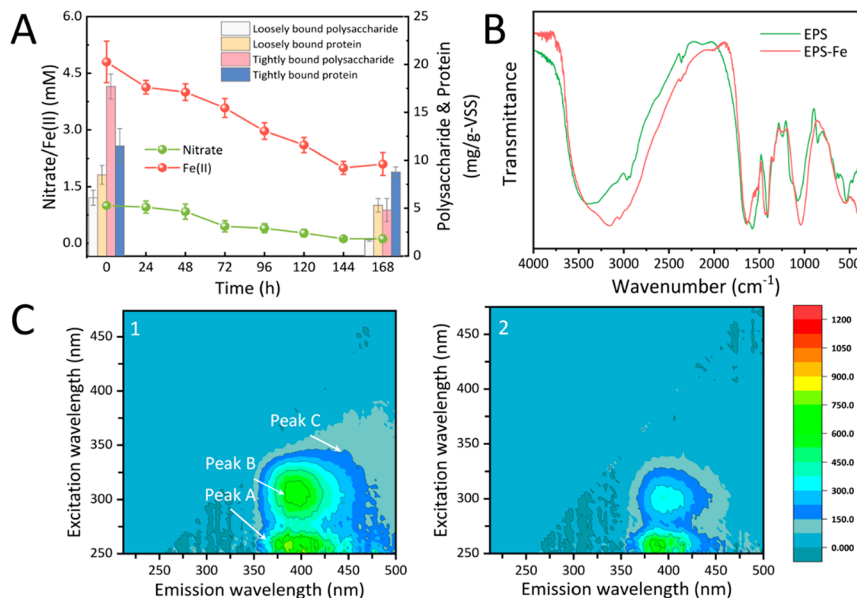


**Figure 2.** Variation in the contents of EPS in the IDAD process (A), FTIR spectra (B), and EEM spectra (C) of EPS before/after the batch tests. Error bars represent the standard deviations of the triplicate batch tests, and asterisks indicate statistical differences ( $p < 0.05$ ) from the origin.

potential formation of cell–iron mineral aggregates and their effects on IDAD activity, cyclic batch tests were carried out, and the denitrification efficiency was continuously measured.

Figure 1 illustrates a continuous decrease in the denitrification efficiency of IDAD sludge after four cycles of cultivation (Figure 1A, B). In the first cycle, the nitrate reduction coupled with Fe(II) oxidation was observed in the IDAD system with a consumed molar ratio of approximately 0.23 (reduced nitrate of 0.8 mM; oxidized Fe(II) of 3.5 mM), which is close to the ideal stoichiometry of the electrons required from Fe(II) to reduce nitrate given in reaction 1. Accordingly, the XRD pattern of the iron-oxidizing products indicates an obvious crystalline structure of lepidocrocite ( $\gamma$ -FeOOH, PDF#08-0098) as one of the primary iron-bearing minerals (Figure S2). However, in cycle 4, only 20% of the initial nitrate was converted with a nitrate reduction rate of 0.003 mM/h, which is 33.3% of the rate measured in cycle 1 (Figure S3). Moreover, the measured ratio of the reacted  $\text{NO}_3^-$ -N to Fe(II) also dropped to 0.17. One reasonable explanation might be that the accumulated Fe(II)-oxidizing products in the IDAD sludge adsorbed a certain amount of Fe(II) species, causing a difference between the actually consumed Fe(II) by the denitrifiers and the measured data. In addition, there was no observable nitrite detected in the whole cyclic cultivation. This result might be ascribed to the notable higher enzymatic activity of the nitrite reductase than that of the nitrate reductase of the IDAD sludge, which led to no nitrite accumulation in the cultivation systems.<sup>11,15</sup>

To obtain a clearly delineated image of such an association, an inverted optical microscope (U-SRE-2, Olympus Co., Japan) was used to observe the formation of cell–iron mineral aggregates. As shown in the microscopy images, the bright-yellow IDAD sludge turned into reddish-brown aggregates along with the Fe(II) oxidation from cycle 1 to cycle 4 (Figure 1C). The color changes of the IDAD sludge indicate a continuous growth of Fe(III) minerals, which might act as substances to adsorb or trap free microbial cells. The SEM image of the IDAD sludge withdrawn at the end of cycle 4 further confirms the association of microbial cells with Fe(III).

precipitates (Figure 1C). Although iron (oxyhydr)oxides serving as attachment carriers for biomass growth were well documented,<sup>38,39</sup> being enwrapped by iron minerals would no doubt hinder the uptake of nutrients and the efflux of adverse metabolites by microorganisms.<sup>22,24,27</sup> Thus, the aggregation of microbes and iron minerals is expected to inhibit the metabolic activity of IDAD sludge (Figure 1D).

**Role of EPS in Cell–Iron Mineral Associations.** EPS, mucilaginous matrixes, play a crucial role in protecting microbial cells from toxic substances, such as heavy metals and nanoparticles.<sup>40</sup> In previous studies of mixotrophic nitrate-reducing Fe(II)-oxidizing microorganisms, a very pronounced EPS envelope around Fe(II)-cultured cells was observed, which was recognized as a responding strategy for preventing cell encrustation.<sup>22,41</sup> In the chemoautotrophic enrichment culture KS and the acclimated iron-dependent denitrifying sludge, EPS were also found closely associated with the mineral particles formed in Fe(II) oxidation.<sup>19,24</sup> Thus, the potential role of EPS in cell–iron mineral associations was further investigated in this work. Figure 2A illustrates the variation of EPS contents in a batch test. Along with oxidation of Fe(II), the EPS contents (both the loosely/tightly bound polysaccharides and proteins) at the end of the batch test showed a significant decrease compared to the initially measured data. To evaluate the potential interference of Fe(III) complexation to the EPS measurement, a preliminary assay of EPS contents at different Fe(III) dosing levels was performed, and no impact of Fe(III) complexation on the EPS measurement was observed (Figure S4). This result is in accordance with our previous findings,<sup>15</sup> which indicates the formation of complexes of EPS and iron minerals.

To get insights into the binding between EPS and iron species, FTIR and EEM measurements were carried out to explore the complexation mechanism. The FTIR spectra of the EPS and EPS–Fe complex are illustrated in Figure 2B. The band around 3400 cm<sup>-1</sup> was the stretching vibration of O–H.<sup>42</sup> Infrared bands at 1649 and 1574 cm<sup>-1</sup> were associated with the C=O stretching (amide I) and C–N stretching and the N–H bending (amide II) in proteins, while the band near

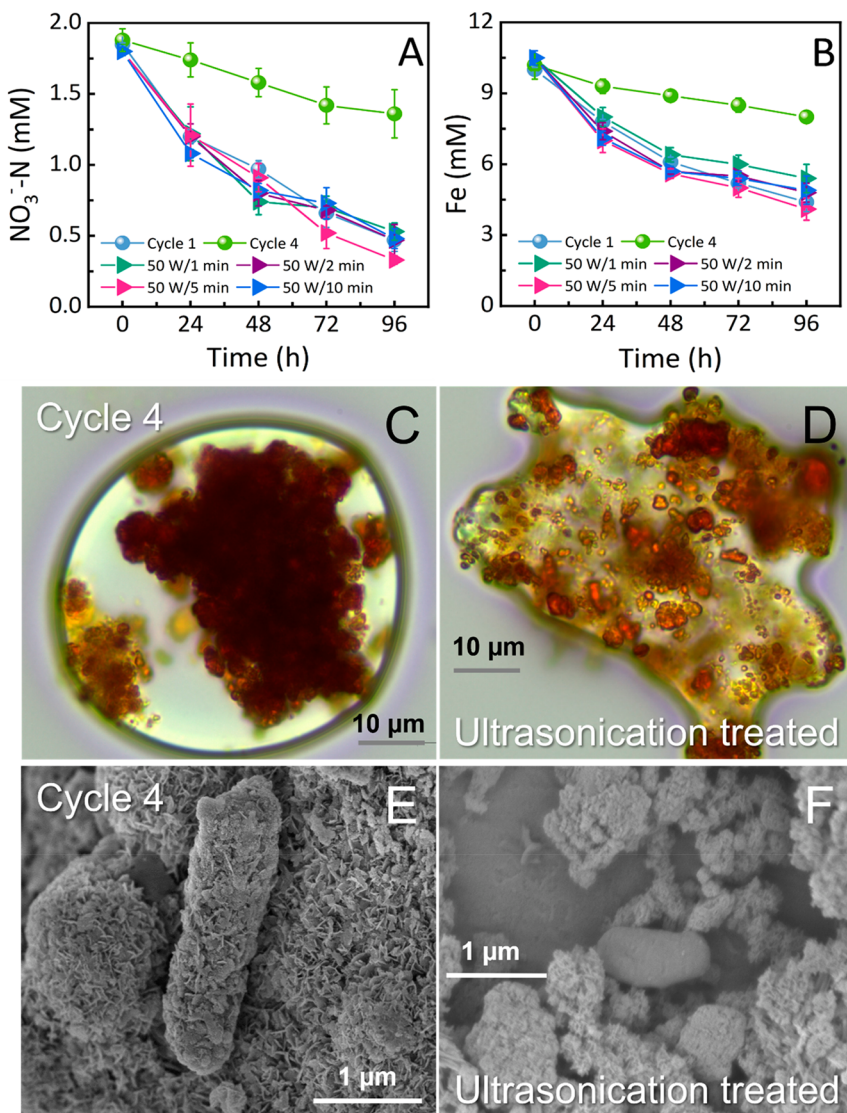


**Figure 3.** Activity recovery of the IDAD sludge after four cycles of cultivation through low-intensity ultrasound treatment (A, B). Microscopy/SEM images of the IDAD sludge after cycle 4 (C, E) and ultrasonic treatment (D, F). Error bars represent the standard deviations of the triplicate batch tests.

1402  $\text{cm}^{-1}$  corresponded to the symmetric stretching of  $\text{C}=\text{O}$  from carboxylic group.<sup>43</sup> A weak adsorption band at 1250  $\text{cm}^{-1}$  was mainly assigned to the deformation vibration of  $\text{C}-\text{O}$  from the carboxylic group and the stretching vibration of the  $\text{P}=\text{O}$  group, while the band at 1080  $\text{cm}^{-1}$  originated from the stretching vibration of  $\text{O}-\text{H}$ .<sup>44</sup> In addition, a minor band at 1137  $\text{cm}^{-1}$  was attributed to  $\text{P}=\text{O}$  stretching.<sup>45</sup> The bands between 650 and 610  $\text{cm}^{-1}$  mainly belonged to the torsional vibration of  $\text{COO}^-$  in lipids.<sup>46</sup>

The EPS–Fe complex showed different spectra compared to those of the initial EPS. The broad bands around 3400  $\text{cm}^{-1}$  and the band at 1080  $\text{cm}^{-1}$  shifted to 3155 and 1040  $\text{cm}^{-1}$ , respectively, and their intensities were substantially enhanced, which was induced by the strong coordination of EPS–Fe. The Infrared band at 1574  $\text{cm}^{-1}$  disappeared, and the intensity of the band at 1402  $\text{cm}^{-1}$  declined. Similar results were obtained when EPS were treated with either copper ions<sup>44</sup> or  $\alpha\text{-Fe}_2\text{O}_3$  particles,<sup>45</sup> suggesting that Fe might bind with the carboxyl groups in EPS. In addition, the bands at 1250 and 1137  $\text{cm}^{-1}$

corresponding to  $\text{P}=\text{O}$  stretching also disappeared, implying the binding of phosphonic groups to Fe.

As shown in Figure 2C, the EEM fluorescence spectra of the EPS were greatly influenced by Fe(II) oxidation. From the EEM data, three peaks were readily identified at excitation/emission ( $\text{Ex}/\text{Em}$ ): 260–270/350–360 nm (peak A), 300–320/360–380 nm (peak B), and 340–360/435–445 nm (peak C) (Figure 2C). Peaks A and B were associated with the aromatic protein-like and tryptophan protein-like substances, while peak C was attributed to the humic acid-like substances.<sup>47,48</sup> The fluorescence intensities of these three peaks were weakened after Fe(II) oxidation. The quenching of fluorophore in EPS by heavy metals was also observed previously,<sup>44,49</sup> indicating a possible structure change of the fluorophores and a tight binding of iron species onto these molecules.

Similar results were obtained when activated sludge was used as the inoculum. Figure S5 illustrates a simultaneous nitrate reduction coupled to Fe(II) oxidation by activated sludge. This result was congruent with previous findings that

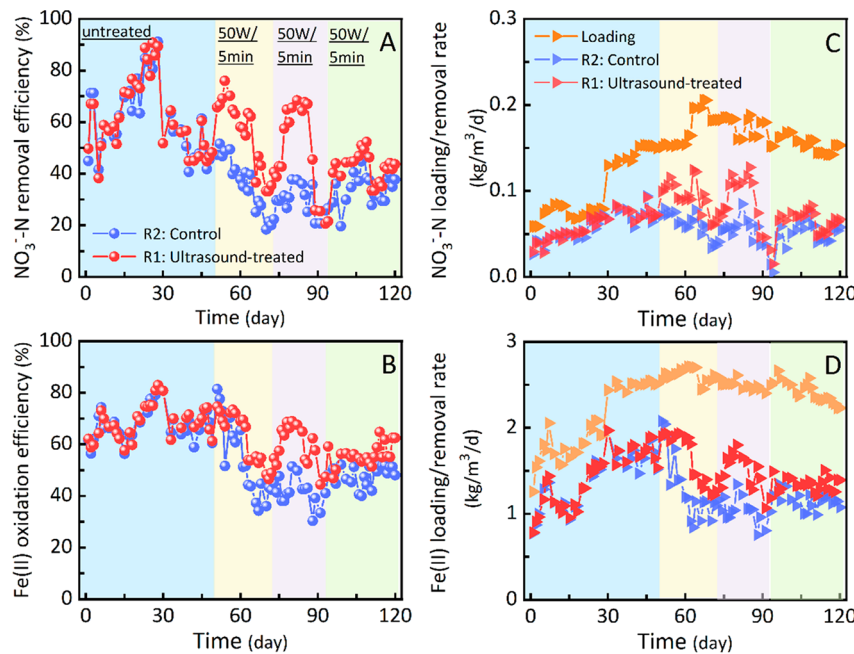


**Figure 4.** Performance of the low-intensity ultrasound-assisted IDAD bioreactor (R1, ultrasound-treated reactor; R2, control reactor). (A) Nitrate in the influent and effluent, (B) nitrate loading/removal rate, (C) Fe(II) in the influent and effluent, and (D) Fe(II) loading/removal rate.

the heterotrophic denitrifying sludge could chemically oxidize Fe(II) by reactive nitrogen species, for example, nitrite.<sup>20,21</sup> An obvious color change from neutral gray to brownish red was observed (Figure S6A), implying the production of Fe(III)-bearing minerals. In the meantime, the sludge–iron mineral aggregates were also observed under a microscope view (Figure S6B, C). In the presence of Fe(II), both the loosely and tightly bound EPS showed a much more significant decreasing trend in comparison to those without Fe(II) (Figure S7A, B). Comparisons between the FTIR spectra of the EPS and EPS–Fe complex also illustrate a shift of the bands corresponding to the O–H stretching near 3430 to 3407 cm<sup>−1</sup>. In addition, these bands and the band at 1080 cm<sup>−1</sup> were largely enhanced. By contrast, the band mainly belonging to the P=O stretching disappeared (Figure S7C, D). A continuous fluorescent quenching of both the protein-like and humic acid-like substances over time was also found in the EEM fluorescence spectra of EPS (Figure S7E–H), which coincided with the observations obtained in the batch test with IDAD sludge. Taken together, these results corroborate that the EPS secreted by the microorganisms could combine with iron species in Fe(II) oxidation, and they were proposed to play a glue-like role in the microbial adhesion onto iron minerals and the formation of cell–iron mineral aggregates.

**Activity Recovery of IDAD Sludge after Ultrasonic Treatment.** To disrupt the cell–iron mineral aggregates, low-intensity ultrasound treatment was adopted after a four cycles of cultivation to recover the activity of IDAD sludge. At given irradiation durations (1, 2, 5, and 10 min), the experimental groups exhibited a complete recovery in terms of the nitrate reduction rate compared to the data obtained in cycle 1 (Figure 3). In addition, the microscopy images of the IDAD sludge before/after ultrasonic treatment show an obvious disruption of the relatively larger aggregates into much smaller ones (Figure 3C, D). Along with the disruption of the reddish-brown aggregates, a crowd of light-colored particles (like the fresh IDAD sludge in Figure 1C) appeared, indicating that the

low-intensity ultrasound treatment disintegrated the cell–iron mineral aggregates. The SEM images also depict that the rough mineral-enwrapped surface of cells turned relatively smooth, which might be ascribed to the stripping of Fe(III) minerals from the cell surface (Figure 3E, F). These results indicate that the observed inhibition on the nitrate reduction along with Fe(II) oxidation was reversible. Although the existence of cell encrustation (periplasmic or cytoplasmic iron oxidation by reactive nitrogen species) in the IDAD system could not be fully ruled out, the recovery of IDAD activity suggests that the aggregation of microbial cells and iron-bearing minerals was the primary cause of the reversible inhibition.

Previous studies on low-intensity ultrasound-assisted biological wastewater treatment underscored an enhanced microbial activity under ultrasonic conditions.<sup>31,32,50</sup> Herein, to comprehensively evaluate whether the metabolic activity of IDAD sludge was stimulated, the effect of ultrasonic treatment on a fresh IDAD sludge was investigated as a compared amendment. After ultrasonic treatment, the denitrification efficiency of the fresh IDAD sludge remained relatively unchanged (Figure S8), suggesting that its activity was neither enhanced nor suppressed by the low-intensity ultrasound. Thus, the recovery of IDAD activity after four cycles of cultivation under ultrasonic conditions was mainly ascribed to the disintegration of the cell–iron mineral aggregates.

**Long-Term Performance of Low-Intensity Ultrasound-Assisted IDAD Bioreactor.** Although the ultrasonic treatment was found to effectively restore the IDAD activity from the cell–iron mineral aggregation-induced inhibition, its effectiveness on the long-term performance of IDAD process was still concealed. Therefore, this work built two identical IDAD bioreactors to further evaluate the potential assistance of low intensity ultrasonication to enhance the operational stability of IDAD process (Figure 4). The two reactors showed similar nitrogen removal performances in phase I (from day 1 to day 50). At a nitrate loading rate of 0.15 kg-N/m<sup>3</sup>/d, a nitrate removal rate of approximately 0.07 kg-N/m<sup>3</sup>/d was

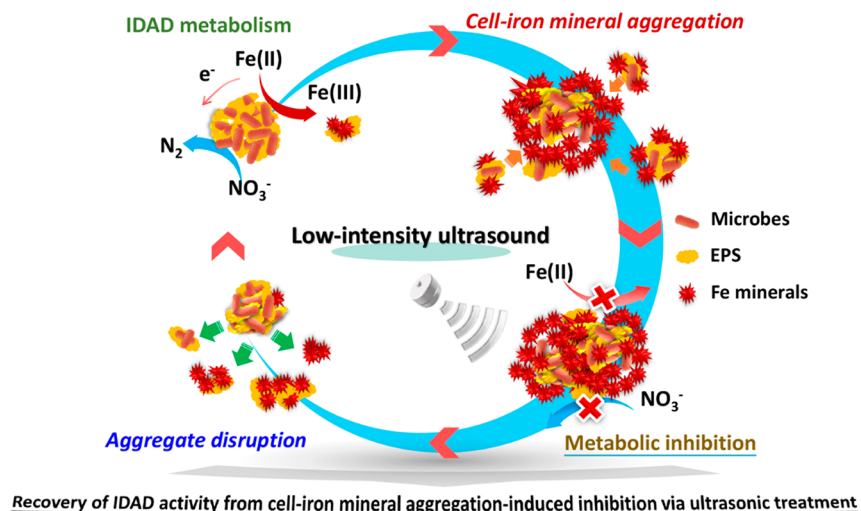


**Figure 5.** Proposed reversible inhibition of cell–iron mineral aggregation on IDAD activity based on its recovery after low-intensity ultrasound treatment.

achieved for both reactors with a nitrogen removal efficiency of 53.3%. When R1 was treated with low-intensity (50 W) ultrasound for 5 min in phase II, its nitrogen removal efficiency remained relatively stable compared to that of the control (R2). In this phase, the average nitrogen removal efficiency of R2 showed a continued decrease to 35.3%. Such a deteriorative trend was also reported previously,<sup>18</sup> which was mainly caused by the accumulation of the Fe(II)-oxidizing products and the aggregation of these minerals and microbial cells in bioreactors.

It should be noted that R1 also exhibited a stepwise declining trend from 64.3% (in the initial two weeks of phase II) to 39.0% (in last 10 days of phase II), suggesting that the ultrasonic treatment did not possess a permanent effectiveness. This result was congruent with the findings in the batch tests, which corroborated that the sonication restored the IDAD activity prominently through breaking the cell–iron mineral aggregates, rather than stimulating the microbial metabolic activity. To further verify this deduction, another run of sonication was immediately applied to R1 when its nitrogen removal efficiency dropped close to that of R2 (phase III). Concomitantly, the nitrogen removal efficiency of R1 rose successively with the highest efficiency of approximately 68.4% in the initial 10 days, but then it decayed rapidly. As the performance of both R1 and R2 steadily deteriorated at the end of phase III, ultrasonic treatment was applied to these two reactors with no distinction (phase IV). Again, the sonication was found effective in improving the performance of the IDAD process as the average nitrogen removal efficiencies of both R1 and R2 in this phase were considerably enhanced compared to those in Phase III.

## ■ DISCUSSION

Operational stability is one of the key issues in wastewater treatment processes. Although IDAD offers several advantages over conventional heterotrophic denitrification, the performance deterioration in a long-term operation is still a Gordian knot in the application of IDAD process.<sup>15,18</sup> To date, cell encrustation during iron oxidation is presumably considered as the main inhibitory effect on the metabolic activity of IDAD sludge, but this argument seems to be particularly feeble based on the findings by Nordhoff et al.<sup>24</sup> Unlike the mixotrophic Fe(II)-oxidizing denitrifiers that suffer from encrustation

caused by the Fe(III) precipitation within the periplasm,<sup>22,41,51</sup> the exclusive iron oxidation coupled to nitrate reduction by the enrichment culture KS proceeds without cell encrustation.<sup>24</sup> The similar community structure of the microbial consortia acclimated from activated sludge in the IDAD-related researches,<sup>15,18,19</sup> the cell encrustation, cannot be or at least should not be regarded as the primary cause of the deterioration of IDAD process.

EPS are mucilaginous matrixes of large polymeric molecules including proteins, polysaccharides, humic acids, nucleic acids, and lipids and are substantiated to play crucial roles in maintaining many essential properties of microbial aggregates.<sup>40,52</sup> Since EPS are rich in ionic functional groups, such as hydroxyl, carboxyl, phosphonic, and amine groups,<sup>53</sup> the glue-like EPS are inevitably bound to iron species as confirmed by the FTIR and EEM results in Fe(II) oxidation, forming cell–iron mineral aggregates. Along with the continuous oxidation of the feeding Fe(II) in the IDAD bioreactor, these aggregates are further combined together to form relatively larger-sized aggregates, where microbial cells are caged, their nutritional pathways blocked, and metabolic activity eventually suppressed (Figure 5). The inhibition caused by cell–iron mineral aggregation was found depending on the accumulation of Fe(III) precipitates; namely, a longer operational duration resulted in a severer inhibition (Figure 1). Moreover, this inhibition was reversible under the experimental conditions, which is supported by the evidence that after sonication, the activity of IDAD sludge was effectively restored compared with its original activity (Figure 3).

Previous studies have documented that sonication (with a common power input range from 100 to 150 J/mL) is an effective means for bound EPS extraction.<sup>52,54,55</sup> Sonication induces the deformation and disruption of the EPS matrix through mechanical vibration with minimized cell lysis.<sup>52</sup> In the IDAD process, when the mucilaginous EPS matrix are bound to iron species, the viscosity of the EPS–Fe complex is decreased, but its solidity is enhanced. As a result, the mechanical vibration produced by sonication is more potent in disrupting these cell–iron mineral aggregates and bring the IDAD bioreactor with high-performance back again (Figure 5). With a fixed intensity, a higher energy input (a longer ultrasonic duration) could produce more EPS extracts.<sup>56,57</sup> In

this work, the ultrasound intensity was controlled at 50 W, and accordingly, the energy input was calculated as 30 to 300 J/mL in the batch tests and approximately 20 J/mL in the continuous reactors. This energy input was far below the critical level (beyond 780 J/mL) that could induce cell lysis.<sup>56</sup>

Low-intensity ultrasound treatment was previously reported to promote the metabolic activity of several typical nitrogen-related microorganisms,<sup>32,58</sup> and it could even affect the microbial community structure in a functional biosystem.<sup>32</sup> However, this work found no observable change in the metabolic rate of IDAD sludge under ultrasonic conditions. It should be noted that the ultrasonic intensity was fixed at 50 W, and only time duration was altered during the assay of IDAD activity in this work. Considering this situation, whether a further promotion of ultrasonic intensity could enhance the metabolic activity of IDAD sludge is unclear yet, which warrants further investigations. The intermittent sonication of 5 min could maintain a stable operation of IDAD bioreactors for approximately 2 weeks. After that, its nitrogen removal performance gradually deteriorated as the Fe(III) precipitates accumulated again (Figure 4). This result underscores that the sonication restored the activity of the IDAD sludge through breaking the cell–iron mineral aggregates, rather than enhancing its metabolic rate. However, the reaggregation of microbes with the residual Fe(III) precipitates in the IDAD system also left a challenge for achieving a permanent effectiveness of the ultrasonic treatment.

In addition, further efforts are required to uprate the nitrogen removal performance of the low-intensity ultrasound-assisted IDAD bioreactor. In this work, the average nitrogen removal efficiency of R1 during the whole operation period was approximately 53.7%. When the cell–iron mineral aggregates were broken, the unintended washout of IDAD sludge resulted in a relatively low biomass retained in the bioreactor, which was a probable cause. By adopting a backflow unit to improve the biomass level within the IDAD bioreactor seems to be a feasible approach. In the meantime, before pumping the washed-out sludge back into the bioreactors, an appropriate separation process, for example, fractional precipitation or magnetic separation, for recovering iron-bearing minerals should also be designed and applied. Strategies for this purpose are not only beneficial for the iron species recovery from the IDAD process but also conducive to effective promotion of the ultrasonic treatment.

**Implications of This Work.** To date, the most important problem that limits the development of an IDAD process is the performance deterioration during long-term operation. Therefore, understanding the hidden cause for this deterioration and exploring the potential solution will no doubt inspire researchers to develop IDAD processes that can be viably controlled and applied. This work demonstrates that cell–iron mineral aggregation, rather than cell encrustation, is the primary cause for the performance deterioration in IDAD process. EPS play a glue-like role in the aggregation of microbial cells and Fe(III) minerals, which enwrap the cells and block their nutritional metabolic pathways, causing reversible inhibition on the activity of IDAD sludge. Adopting low-intensity ultrasound treatment could effectively break such aggregates, free microbial cells, and restore IDAD activity. In addition, the low intensity ultrasonication-assisted IDAD bioreactor also showed a relatively stable operational performance compared to the control one. Currently, ultrasonic equipment for sludge treatment is commercially available,

which makes it feasible to magnify this process to pilot- and full-scale implementations. The findings of this work may boost the development of IDAD processes toward industrialized application. Thus, further investigations into the economical assessment of ultrasonication and the optimization of other operational factors (e.g., specific energy input and ultrasonic frequency) should be considered.

## ASSOCIATED CONTENT

### Supporting Information

The Supporting Information is available free of charge at <https://pubs.acs.org/doi/10.1021/acs.est.1c05553>.

Additional table describing four operational phases of IDAD bioreactors (Table S1). Additional figures of schematic diagram of bench-scale low-intensity ultrasound-assisted IDAD bioreactors (Figure S1). XRD pattern of the iron-oxidizing products (Figure S2). Loss of nitrogen removal activity of IDAD sludge (Figure S3). Effect of Fe(III) on EPS determination (Figure S4). Nitrate reduction coupled to Fe(II) oxidation by activated sludge (Figure S5). Morphological changes of activated sludge after Fe(II) oxidation (Figure S6). Variation of EPS in a batch test with activated sludge as inoculum, FT-IR spectra and EEM spectra of EPS before/after the batch test (Figure S7), and effect of low-intensity ultrasound treatment on IDAD activity (Figure S8) ([PDF](#))

## AUTHOR INFORMATION

### Corresponding Author

Han-Qing Yu – CAS Key Laboratory of Urban Pollutant Conversion, Department of Environmental Science and Engineering, University of Science and Technology of China, Hefei 230026, China; School of Resources and Environmental Engineering, Hefei University of Technology, Hefei 230009, China; [orcid.org/0000-0001-5247-6244](#); Email: [hqyu@ustc.edu.cn](mailto:hqyu@ustc.edu.cn); Fax: +86-551-63601592

### Authors

Tian Tian – CAS Key Laboratory of Urban Pollutant Conversion, Department of Environmental Science and Engineering, University of Science and Technology of China, Hefei 230026, China; Key Laboratory of Industrial Ecology and Environmental Engineering (Ministry of Education, China), School of Environmental Science and Technology, Dalian University of Technology, Dalian 116024, China; [orcid.org/0000-0002-6137-305X](#)

Ke Zhou – School of Resources and Environmental Engineering, Hefei University of Technology, Hefei 230009, China

Yu-Sheng Li – CAS Key Laboratory of Urban Pollutant Conversion, Department of Environmental Science and Engineering, University of Science and Technology of China, Hefei 230026, China

Dong-Feng Liu – CAS Key Laboratory of Urban Pollutant Conversion, Department of Environmental Science and Engineering, University of Science and Technology of China, Hefei 230026, China; [orcid.org/0000-0002-5954-6476](#)

Complete contact information is available at:  
<https://pubs.acs.org/doi/10.1021/acs.est.1c05553>

**Notes**

The authors declare no competing financial interest.

**ACKNOWLEDGMENTS**

The authors wish to thank the National Natural Science Foundation of China (51908529 and 51821006), the Anhui Provincial Natural Science Foundation (1908085QB88), the China Postdoctoral Science Foundation (2018M642543), and the Fundamental Research Funds for the Central Universities (DUT20RC(3)093) for supporting this work.

**REFERENCES**

- (1) Tagliabue, A.; Bowie, A. R.; Boyd, P. W.; Buck, K. N.; Johnson, K. S.; Saito, M. A. The integral role of iron in ocean biogeochemistry. *Nature* **2017**, *543* (7643), 51–59.
- (2) Bryce, C.; Blackwell, N.; Schmidt, C.; Otte, J.; Huang, Y.; Kleindienst, S.; Tomaszewski, E.; Schad, M.; Warter, V.; Peng, C.; Byrne, J. M.; Kappler, A. Microbial anaerobic Fe(II) oxidation – ecology, mechanisms and environmental implications. *Environ. Microbiol.* **2018**, *20* (10), 3462–3483.
- (3) Laufer, K.; Røy, H.; Jørgensen, B. B.; Kappler, A. Evidence for the existence of autotrophic nitrate-reducing Fe(II)-oxidizing bacteria in marine coastal sediment. *Appl. Environ. Microbiol.* **2016**, *82* (20), 6120–6131.
- (4) Michiels, C. C.; Darchambeau, F.; Roland, F. A. E.; Morana, C.; Llirós, M.; García-Armisen, T.; Thamdrup, B.; Borges, A. V.; Canfield, D. E.; Servais, P.; Desey, J.; Crowe, S. A. Iron-dependent nitrogen cycling in a ferruginous lake and the nutrient status of Proterozoic oceans. *Nat. Geosci.* **2017**, *10*, 217–221.
- (5) Straub, K. L.; Benz, M.; Schink, B.; Widdel, F. Anaerobic, nitrate-dependent microbial oxidation of ferrous iron. *Appl. Environ. Microbiol.* **1996**, *62* (4), 1458–1460.
- (6) Hohmann, C.; Winkler, E.; Morin, G.; Kappler, A. Anaerobic Fe(II)-oxidizing bacteria show As resistance and immobilize As during Fe(III) mineral precipitation. *Environ. Sci. Technol.* **2010**, *44* (1), 94–101.
- (7) Omoregie, E. O.; Couture, R. M.; Van Cappellen, P.; Corkhill, C. L.; Charnock, J. M.; Polya, D. A.; Vaughan, D.; Vanbroekhoven, K.; Lloyd, J. R. Arsenic bioremediation by biogenic iron oxides and sulfides. *Appl. Environ. Microbiol.* **2013**, *79* (14), 4325–4335.
- (8) Sun, J.; Chillrud, S. N.; Mailloux, B. J.; Bostick, B. C. In situ magnetite formation and long-term arsenic immobilization under advective flow conditions. *Environ. Sci. Technol.* **2016**, *50* (18), 10162–10171.
- (9) Jokai, K.; Nakamura, T.; Okabe, S.; Ishii, S. Simultaneous removal of nitrate and heavy metals in a continuous flow nitrate-dependent ferrous iron oxidation (NDOFO) bioreactor. *Chemosphere* **2021**, *262*, 127838.
- (10) Zhu, T. T.; Cheng, H. Y.; Yang, L. H.; Su, S. G.; Wang, H. C.; Wang, S. S.; Wang, A. J. Coupled sulfur and iron(II) carbonate-driven autotrophic denitrification for significantly enhanced nitrate removal. *Environ. Sci. Technol.* **2019**, *53* (3), 1545–1554.
- (11) Tian, T.; Zhou, K.; Li, Y. S.; Liu, D. F.; Yu, H. Q. Phosphorus recovery from wastewater prominently through a Fe(II)-P oxidizing pathway in the autotrophic iron-dependent denitrification process. *Environ. Sci. Technol.* **2020**, *54* (18), 11576–11583.
- (12) He, S. M.; Tominski, C.; Kappler, A.; Behrens, S.; Roden, E. E. Metagenomic analyses of the autotrophic Fe(II)-oxidizing, nitrate-reducing enrichment culture KS. *Appl. Environ. Microbiol.* **2016**, *82* (9), 2656–2668.
- (13) Tominski, C.; Heyer, H.; Lösekann-Behrens, T.; Behrens, S.; Kappler, A. Growth and population dynamics of the anaerobic Fe(II)-oxidizing and nitrate-reducing enrichment culture KS. *Appl. Environ. Microbiol.* **2018**, *84* (9), e02173–17.
- (14) Huang, Y. M.; Straub, D.; Blackwell, N.; Kappler, A.; Kleindienst, S. Meta-omics reveal *Gallionellaceae* and *Rhodanobacter* species as interdependent key players for Fe(II) oxidation and nitrate reduction in the autotrophic enrichment culture KS. *Appl. Environ. Microbiol.* **2021**, *87*, AEM00496.
- (15) Tian, T.; Zhou, K.; Xuan, L.; Zhang, J. X.; Li, Y. S.; Liu, D. F.; Yu, H. Q. Exclusive microbially driven autotrophic iron-dependent denitrification in a reactor inoculated with activated sludge. *Water Res.* **2020**, *170*, 115300.
- (16) Jakus, N.; Blackwell, N.; Osenbrück, K.; Straub, D.; Byrne, J. M.; Wang, Z.; Glöckler, D.; Elsner, M.; Lueders, T.; Grathwohl, P.; Kleindienst, S.; Kappler, A. Nitrate removal by a novel lithoautotrophic nitrate-reducing, iron(II)-oxidizing culture enriched from a pyrite-rich limestone aquifer. *Appl. Environ. Microbiol.* **2021**, *87*, AEM00460.
- (17) Jakus, N.; Mellage, A.; Höschken, C.; Maisch, M.; Byrne, J. M.; Mueller, C. W.; Grathwohl, P.; Kappler, A. Anaerobic neutrophilic pyrite oxidation by a chemolithoautotrophic nitrate-reducing iron(II)-oxidizing culture enriched from a fractured-aquifer. *Environ. Sci. Technol.* **2021**, *55* (14), 9876–9884.
- (18) Wang, R.; Yang, C.; Zhang, M.; Xu, S. Y.; Dai, C. L.; Liang, L. Y.; Zhao, H. P.; Zheng, P. Chemoautotrophic denitrification based on ferrous iron oxidation: Reactor performance and sludge characteristics. *Chem. Eng. J.* **2017**, *313*, 693–701.
- (19) Zhang, M.; Zhangzhu, G. C.; Wen, S. X.; Lu, H. F.; Wang, R.; Li, W.; Ding, S.; Ghulam, A.; Zheng, P. Chemolithotrophic denitrification by nitrate-dependent anaerobic iron oxidizing (NAIO) process: insights into the evaluation of seeding sludge. *Chem. Eng. J.* **2018**, *345*, 345–352.
- (20) Zhang, M.; Zheng, P.; Li, W.; Wang, R.; Ding, S.; Abbas, G. Performance of nitrate-dependent anaerobic ferrous oxidizing (NAFO) process: a novel prospective technology for autotrophic denitrification. *Bioresour. Technol.* **2015**, *179*, 543–548.
- (21) Wang, R.; Zheng, P.; Zhang, M.; Zhao, H. P.; Ji, J. Y.; Zhou, X. X.; Li, W. Bioaugmentation of nitrate-dependent anaerobic ferrous oxidation by heterotrophic denitrifying sludge addition: a promising way for promotion of chemoautotrophic denitrification. *Bioresour. Technol.* **2015**, *197*, 410–415.
- (22) Klueglein, N.; Zeitvogel, F.; Stierhof, Y. D.; Floetenmeyer, M.; Konhauser, K. O.; Kappler, A.; Obst, M. Potential role of nitrite for abiotic Fe(II) oxidation and cell encrustation during nitrate reduction by denitrifying bacteria. *Appl. Environ. Microbiol.* **2014**, *80* (3), 1051–1061.
- (23) Chen, D. D.; Liu, T. X.; Li, X. M.; Li, F. B.; Luo, X. B.; Wu, Y. D.; Wang, Y. Biological and chemical processes of microbially mediated nitrate-reducing Fe(II) oxidation by *Pseudogulbenkiania* sp. strain 2002. *Chem. Geol.* **2018**, *476*, 59–69.
- (24) Nordhoff, M.; Tominski, C.; Halama, M.; Byrne, J. M.; Obst, M.; Kleindienst, S.; Behrens, S.; Kappler, A. Insights into nitrate-reducing Fe(II) oxidation mechanisms through analysis of cell–mineral associations, cell encrustation, and mineralogy in the chemolithoautotrophic enrichment culture KS. *Appl. Environ. Microbiol.* **2017**, *83* (13), e00752.
- (25) Wang, R.; Xu, S. Y.; Zhang, M.; Ghulam, A.; Dai, C. L.; Zheng, P. Iron as electron donor for denitrification: the efficiency, toxicity and mechanism. *Ecotoxicol. Environ. Saf.* **2020**, *194*, 110343.
- (26) Gilmore, B. F.; Flynn, P. B.; O'Brien, S.; Hickok, N.; Freeman, T.; Bourke, P. Cold plasmas for biofilm control: opportunities and challenges. *Trends Biotechnol.* **2018**, *36* (6), 627–638.
- (27) Schadler, S.; Burkhardt, C.; Hegler, F.; Straub, K. L.; Miot, J.; Benzerara, K.; Kappler, A. Formation of cell–iron-mineral aggregates by phototrophic and nitrate-reducing anaerobic Fe(II)-oxidizing bacteria. *Geomicrobiol. J.* **2009**, *26* (2), 93–103.
- (28) Wu, W.; Swanner, E. D.; Hao, L.; Zeitvogel, F.; Obst, M.; Pan, Y.; Kappler, A. Characterization of the physiology and cell–mineral interactions of the marine anoxygenic phototrophic Fe(II) oxidizer *Rhodovulum iodosum* – implications for Precambrian Fe(II) oxidation. *FEMS Microbiol. Ecol.* **2014**, *88* (3), 503–515.
- (29) Yu, G. H.; He, P. J.; Shao, L. M.; Zhu, Y. S. Extracellular proteins, polysaccharides and enzymes impact on sludge aerobic digestion after ultrasonic pretreatment. *Water Res.* **2008**, *42* (8–9), 1925–1934.

- (30) Wang, B. B.; Chang, Q.; Peng, D. C.; Hou, Y. P.; Li, H. J.; Pei, L. Y. A new classification paradigm of extracellular polymeric substances (EPS) in activated sludge: separation and characterization of exopolymers between floc level and microcolony level. *Water Res.* **2014**, *64*, 53–60.
- (31) Dai, C.; Xiong, F.; He, R.; Zhang, W.; Ma, H. Effects of low-intensity ultrasound on the growth, cell membrane permeability and ethanol tolerance of *Saccharomyces cerevisiae*. *Ultrason. Sonochem.* **2017**, *36*, 191–197.
- (32) Zheng, M.; Liu, Y. C.; Xin, J.; Zuo, H.; Wang, C. W.; Wu, W. M. Ultrasonic treatment enhanced ammonia-oxidizing bacterial (AOB) activity for nitritation process. *Environ. Sci. Technol.* **2016**, *50* (2), 864–871.
- (33) Tian, T.; Qiao, S.; Yu, C.; Tian, Y. H.; Yang, Y.; Zhou, J. T. Distinct and diverse anaerobic respiration of methanogenic community in response to MnO<sub>2</sub> nanoparticles in anaerobic digester sludge. *Water Res.* **2017**, *123*, 206–215.
- (34) Qian, C.; Chen, W.; Gong, B.; Yu, H. Q. Determination of saccharides in environments using a sulfuric acid-fluorescence approach. *Environ. Sci. Technol.* **2020**, *54* (11), 6632–6638.
- (35) *Standard Methods for the Examination of Water and Wastewater*, 20th ed.; American Public Health Association: Washington, DC, 1998.
- (36) Klueglein, N.; Picardal, F.; Zedda, M.; Zwiener, C.; Kappler, A. Oxidation of Fe(II)-EDTA by nitrite and by two nitrate-reducing Fe(II)-oxidizing *Acidovorax* strains. *Geobiology* **2015**, *13* (2), 198–207.
- (37) Shrout, J. D.; Williams, A. G.; Scherer, M. M.; Parkin, G. F. Inhibition of bacterial perchlorate reduction by zero-valent iron. *Biodegradation* **2005**, *16* (1), 23–32.
- (38) Dykstra, C. M.; Pavlostathis, S. G. Zero-valent iron enhances biocathodic carbon dioxide reduction to methane. *Environ. Sci. Technol.* **2017**, *51* (21), 12956–12964.
- (39) He, C. S.; He, P. P.; Yang, H. Y.; Li, L. L.; Lin, Y.; Mu, Y.; Yu, H. Q. Impact of zero-valent iron nanoparticles on the activity of anaerobic granular sludge: from macroscopic to microcosmic investigation. *Water Res.* **2017**, *127*, 32–40.
- (40) Tang, J.; Wu, Y.; Esquivel-Elizondo, S.; Sorensen, S. J.; Rittmann, B. E. How microbial aggregates protect against nanoparticle toxicity. *Trends Biotechnol.* **2018**, *36* (11), 1171–1182.
- (41) Schmid, G.; Zeitvogel, F.; Hao, L.; Ingino, P.; Floetenmeyer, M.; Stierhof, Y. D.; Schroepel, B.; Burkhardt, C. J.; Kappler, A.; Obst, M. 3-D analysis of bacterial cell-(iron)mineral aggregates formed during Fe(II) oxidation by the nitrate-reducing *Acidovorax* sp. strain BoFeN1 using complementary microscopy tomography approaches. *Geobiology* **2014**, *12* (4), 340–361.
- (42) Wang, L. L.; Wang, L. F.; Ren, X. M.; Ye, X. D.; Li, W. W.; Yuan, S. J.; Sun, M.; Sheng, G. P.; Yu, H. Q.; Wang, X. K. pH dependence of structure and surface properties of microbial EPS. *Environ. Sci. Technol.* **2012**, *46* (2), 737–744.
- (43) Ha, J.; Gelabert, A.; Spormann, A. M.; Brown, G. E. Role of extracellular polymeric substances in metal ion complexation on *Shewanella oneidensis*: Batch uptake, thermodynamic modeling, ATR-FTIR, and EXAFS study. *Geochim. Cosmochim. Acta* **2010**, *74* (1), 1–15.
- (44) Sheng, G. P.; Xu, J.; Luo, H. W.; Li, W. W.; Li, W. H.; Yu, H. Q.; Xie, Z.; Wei, S. Q.; Hu, F. C. Thermodynamic analysis on the binding of heavy metals onto extracellular polymeric substances (EPS) of activated sludge. *Water Res.* **2013**, *47* (2), 607–614.
- (45) Parikh, S. J.; Chorover, J. ATR-FTIR spectroscopy reveals bond formation during bacterial adhesion to iron oxide. *Langmuir* **2006**, *22* (20), 8492–8500.
- (46) Pandiarajan, S.; Umadevi, M.; Sasirekha, V.; Rajaram, R. K.; Ramakrishnan, V. FT-IR and FT-Raman spectral studies of bis(L-proline) hydrogen nitrate and bis(L-proline) hydrogen perchlorate. *J. Raman Spectrosc.* **2005**, *36* (10), 950–961.
- (47) Chen, W.; Westerhoff, P.; Leenheer, J. A.; Booksh, K. Fluorescence excitation-emission matrix regional integration to quantify spectra for dissolved organic matter. *Environ. Sci. Technol.* **2003**, *37* (24), 5701–5710.
- (48) Chen, W.; Qian, C.; Zhou, K. G.; Yu, H. Q. Molecular spectroscopic characterization of membrane fouling: a critical review. *Chem-US* **2018**, *4* (7), 1492–1509.
- (49) Liu, Y.; Jin, R. F.; Liu, G. F.; Tian, T.; Zhou, J. T. Effects of hexavalent chromium on performance, extracellular polymeric substances and microbial community structure of anaerobic activated sludge in a sequencing batch reactor. *J. Chem. Technol. Biotechnol.* **2017**, *92* (10), 2719–2730.
- (50) Cho, S. K.; Kim, D. H.; Quince, C.; Im, W. T.; Oh, S. E.; Shin, S. G. Low-strength ultrasonication positively affects methanogenic granules toward higher AD performance: implications from microbial community shift. *Ultrason. Sonochem.* **2016**, *32*, 198–203.
- (51) Miot, J.; Remusat, L.; Duprat, E.; Gonzalez, A.; Pont, S.; Poinsot, M. Fe biomineralization mirrors individual metabolic activity in a nitrate-dependent Fe(II)-oxidizer. *Front. Microbiol.* **2015**, *6*, 879.
- (52) Pellicer-Nacher, C.; Domingo-Felez, C.; Mutlu, A. G.; Smets, B. F. Critical assessment of extracellular polymeric substances extraction methods from mixed culture biomass. *Water Res.* **2013**, *47* (15), 5564–5574.
- (53) Liu, J.; Tang, J.; Wan, J.; Wu, C.; Graham, B.; Kerr, P. G.; Wu, Y. Functional sustainability of periphytic biofilms in organic matter and Cu<sup>2+</sup> removal during prolonged exposure to TiO<sub>2</sub> nanoparticles. *J. Hazard. Mater.* **2019**, *370*, 4–12.
- (54) Kang, F.; Alvarez, P. J.; Zhu, D. Microbial extracellular polymeric substances reduce Ag<sup>+</sup> to silver nanoparticles and antagonize bactericidal activity. *Environ. Sci. Technol.* **2014**, *48* (1), 316–322.
- (55) Kuo-Dahab, W. C.; Stauch-White, K.; Butler, C. S.; Gikonyo, G. J.; Carbajal-Gonzalez, B.; Ivanova, A.; Dolan, S.; Park, C. Investigation of the fate and dynamics of extracellular polymeric substances (EPS) during sludge-based photogranulation under hydrostatic conditions. *Environ. Sci. Technol.* **2018**, *52* (18), 10462–10471.
- (56) Han, X. M.; Wang, Z. W.; Zhu, C. W.; Wu, Z. C. Effect of ultrasonic power density on extracting loosely bound and tightly bound extracellular polymeric substances. *Desalination* **2013**, *329*, 35–40.
- (57) Monique, R.; Elisabeth, G. N.; Etienne, P.; Dominique, L. A high yield multi-method extraction protocol for protein quantification in activated sludge. *Bioresour. Technol.* **2008**, *99* (16), 7464–7471.
- (58) Duan, X.; Zhou, J.; Qiao, S.; Wei, H. Application of low intensity ultrasound to enhance the activity of anammox microbial consortium for nitrogen removal. *Bioresour. Technol.* **2011**, *102* (5), 4290–4293.